Large eddy simulations of time-dependent and buoyancy-driven channel flows

By W. Cabot

1. Motivations and objectives

The dynamic subgrid-scale (SGS) model (Germano *et al.*, 1991; Lilly, 1992) has proven successful in the large-eddy simulation (LES) of several simple turbulent flows, e.g., in homogeneous, incompressible flow with passive scalars and homogeneous, compressible flow (Moin *et al.*, 1991); in transitional and steady plane-Pouiseille channel flow (Germano *et al.*, 1991); and in passive scalar transport in channel flow (Cabot, 1991; Cabot & Moin, 1991). The dynamic SGS model, using eddy viscosity and diffusivity models as a basis, determines the spatially and temporally varying coefficients by effectively extrapolating the SGS stress and heat flux from the small, resolved scale structure, thus allowing the SGS model to adapt to temporally varying flow conditions and solid boundaries. In contrast, standard SGS models require tuning of model constants and *ad hoc* damping functions at walls. In order to apply the dynamic SGS model to more complicated turbulent flows that arise in geophysical and astrophysical situations, one needs to determine if the dynamic SGS model can accurately model the effects of subgrid scales in flows with, e.g., thermal convection, compressibility, and rapid uniform or differential rotation.

The primary goal of this work has been to assess the performance of the dynamic SGS model in the LES of channel flows in a variety of situations, viz., in temporal development of channel flow turned by a transverse pressure gradient and especially in buoyancy-driven turbulent flows such as Rayleigh-Bénard and internally heated channel convection. For buoyancy-driven flows, there are additional buoyant terms that are possible in the base models, and one objective has been to determine if the dynamic SGS model results are sensitive to such terms. The ultimate goal is to determine the minimal base model needed in the dynamic SGS model to provide accurate results in flows with more complicated physical features. In addition, a program of direct numerical simulation (DNS) of fully compressible channel convection has been undertaken to determine stratification and compressibility effects. These simulations are intended to provide a comparative base for performing the LES of compressible (or highly stratified, pseudo-compressible) convection at high Reynolds number in the future.

2. Accomplishments

2.1 Large eddy simulation of time-dependent channel flow

The dynamic SGS model was used in the LES of fully turbulent channel flow driven by a uniform streamwise (x) pressure gradient that is suddenly turned by a transverse (z) pressure gradient 10 times larger. The DNS of this case was performed by Moin *et al.* (1990). They found, counterintuitively but consistent with

experimental results of three dimensional boundary layers, that the turbulence kinetic energy and shear production rate initially decrease and later recover. Until Durbin (1992, and in this volume), no Reynolds averaged type model had been able to reproduce this behavior.

The LES was performed with a spectral-Chebyshev code (Kim *et al.*, 1987) on a $32 \times 65 \times 32$ mesh in a $4\pi \times 2 \times 4\pi/3$ box (in units of channel half-width δ). The dynamic SGS model used a ratio of test to grid filter widths of 2 in the horizontal directions (using a sharp spectral-cutoff filter) and 1 in the normal (y) direction (i.e., no explicit filtering in y). Defining the effective filter width as $\Delta = (\Delta_x \Delta_y \Delta_z)^{1/3}$ gives a test to grid effective filter width ratio $\widehat{\Delta}/\Delta = 2^{2/3}$. A Smagorinsky (1963) eddy viscosity base model was used whose coefficient, assumed to be a function of y and time, was calculated at each time step by averaging over horizontal planes (see Cabot, 1991). An ensemble of temporally developing flows was approximated by initially generating 15 fully developed turbulent channel flow fields separated in time by a sufficient amount to make them statistically independent. The initial channel flow fields were developed for a friction Reynolds number ($Re_\tau = u_{\tau o}\delta/\nu$, where $u_{\tau o}$ is the initial friction speed and ν is the molecular viscosity) of 180. The 15 fields were simultaneously advanced in time from $t = 0$ to 1.2 (in units of $\delta/u_{\tau o}$), and statistics were generated for each field every Δt of 0.15 and averaged together. The statistics from this LES were in good qualitative and quantitative agreement with those from the DNS (Moin *et al.*, 1990), although the recovery in the turbulence kinetic energy in the LES occurred at a slightly later time than in the DNS.

To test if it was the SGS model that was responsible for these good results in the LES or if it was due merely to an accurate portrayal of the large-scale interactions, a DNS was computed on the same coarse grid. The initial fields for the time-dependent calculation were first run to statistical equilibrium on the coarse grid, rather than simply turning off the SGS model in the LES initial fields, in order to avoid spurious transients due to the sudden drop in effective viscosity. The initial statistics for the coarse DNS and LES cases are thus not the same. The results of the coarse DNS were for the most part found to be in qualitative agreement with the well resolved DNS results of Moin *et al.* (1990), but the quantitative agreement was substantially poorer than was found using the dynamic SGS model. Thus much of the "three-dimensional" response of the turned channel flow is contained in the large-scale interactions, but the finer details require the SGS model. The greatest disagreement was found in the temporal behavior of the total (resolved and SGS) dissipation rate (Figure 1), which is to be expected since it depends to a larger extent on the different treatment of the small scales. In the DNS of Moin *et al.* (1990) and the LES, the dissipation rate has a complicated behavior near the wall, initially decreasing at the wall but increasing farther out in the near-wall region; the wall dissipation eventually begins to recover at $t = 1.2$. In the coarse DNS, however, the dissipation rate (which begins at a substantially higher level at the wall than in the LES) decreases both at the wall and in the near-wall region with no sign of recovery at $t = 1.2$. Such inaccuracies in the energy rates likely lead to the quantitative discrepancies in the velocity statistics.

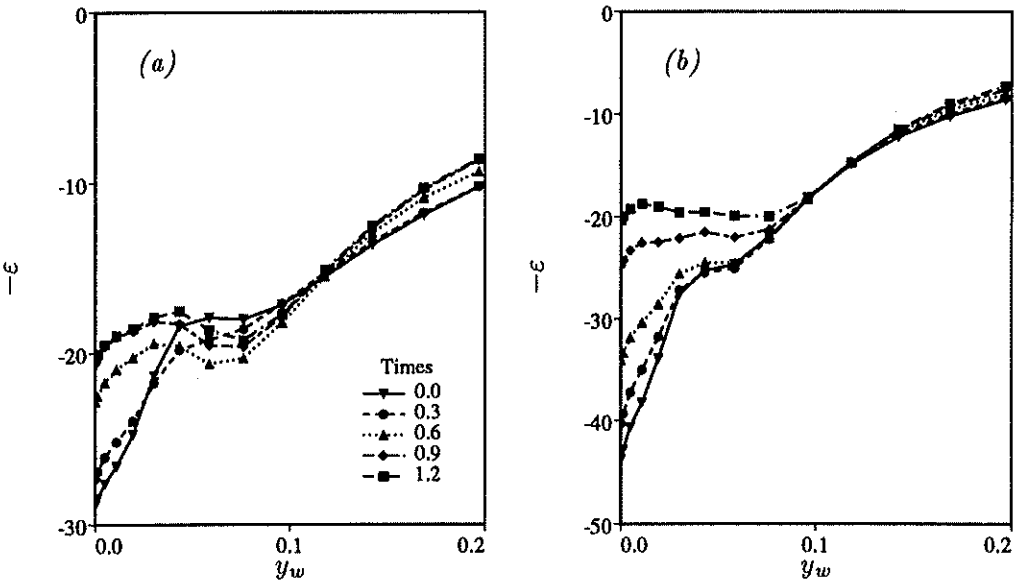

FIGURE 1. Total dissipation rates near the wall (plotted as the distance from the wall in units of δ) for channel flow turned by a transverse pressure gradient. (a) LES using the dynamic SGS model; (b) coarse DNS computed on the same grid.

2.2 Large eddy simulation of thermal convection

2.2.1 Base models

Simple eddy viscosity and diffusivity SGS models, with some near-wall corrections, are commonly used in the LES of thermal convection (see Nieuwstadt, 1990, for a recent review). Some modelers employ additional buoyancy corrections (e.g., Eidson, 1985; Mason, 1989; Schumann, 1991). The eddy viscosity and diffusivity models that I have used to date as the basis for the dynamic SGS procedure can be generalized in a form similar to Schumann's (1991) "first-order" SGS model, which is a vast simplification of more general, second-order, Reynolds-stress-like equations. The model for the residual SGS Reynolds stress at an arbitrary filter level is

$$\tau - \tfrac{1}{3}\mathrm{Tr}(\tau)\mathbf{I} = -2\nu_t\mathbf{S} = -2C_\nu\Delta^2\sigma\mathbf{S}\,, \tag{1}$$

where $\mathbf{I}$ is the identity tensor, C_ν is the coefficient of the eddy viscosity ν_t, Δ is the effective filter width, and $\mathbf{S}$ is the strain rate tensor; σ is a scale rate defined below. The residual heat (or scalar) flux is modeled by

$$\mathbf{h} = -C_\alpha\Delta^2\sigma\mathcal{B}\cdot\nabla\theta\,, \quad \mathcal{B} = \mathbf{I} + c_2\beta\nabla\theta/(\sigma^2 - c_2N_c^2)\,, \tag{2}$$

where C_α is the eddy diffusivity coefficient, θ is the potential temperature, β is the buoyancy vector (gravity times thermal expansion coefficient), and $N_c^2 = \beta\cdot\nabla\theta$. The scale rate σ is given, from SGS energy production = dissipation arguments, by

$$\sigma^2 = \tfrac{1}{2}\left[S^2 + (c_1+c_2)N_c^2\right] + \left\{\tfrac{1}{4}\left[S^2 + (c_1-c_2)N_c^2\right]^2 + c_1c_2N_m^4\right\}^{1/2}, \tag{3}$$

where $S^2 = 2\mathbf{S} : \mathbf{S}$ and $N_m^4 = (\boldsymbol{\beta} \cdot \boldsymbol{\beta})(\nabla\theta \cdot \nabla\theta)$. The constant or coefficient c_1 is, in principle, $C_\alpha/C_\nu = 1/\mathrm{Pr}_t$; c_2 is, in principle, related to the ratio of turbulent time scales of the velocity and potential temperature. Notice that (3) reduces to the normal Smagorinsky model scaling ($\sigma = S$) for no buoyancy ($\boldsymbol{\beta} = 0$) and that σ^2 and $\sigma^2 - c_2 N_c^2$ are positive semi-definite if $c_1 c_2 \geq 0$. Also notice that the residual heat flux in (2) is anisotropic with respect to $\nabla\theta$ for finite c_2 and $\boldsymbol{\beta}$, being enhanced in the direction of buoyancy forces. (Analogous anisotropic terms could be included in (1) by replacing $\mathbf{S}$ by $\boldsymbol{\mathcal{B}} \cdot \mathbf{S}$; but Schumann (1991) found that they led to realizability problems in his LES and so advocates dropping them.) For $c_2 = 0$, we can identify $\mathbf{h}$ with $-\alpha_t \nabla\theta$, where α_t is the eddy diffusivity.

The differences in the base models arise from different treatments of c_1 and c_2:

A. The "scalar" model has $c_1 = c_2 = 0$. C_ν and C_α are determined as functions of y and t by the dynamic test-filtering procedure. This is the model for the dynamic SGS model employed by Moin *et al.* (1991) and Cabot & Moin (1991). I have applied it to Rayleigh-Bénard convection.

B. The "buoyancy" model has c_1 as a coefficient equated consistently with $C_\alpha/C_\nu = 1/\mathrm{Pr}_t$ and $c_2 = 0$ (isotropic eddy diffusivity). This requires an iterative solution of the eddy coefficients (Cabot, 1991) with a Newton's (secant) method. It has been applied to Rayleigh-Bénard convection and low-Pr internally heated channel convection.

C. The "Eidson" model, after Eidson's (1985) SGS model, is the same as B but with c_1 taken as a constant (2.5) corresponding to his best value of $\mathrm{Pr}_t = 0.4$ for the LES of Rayleigh-Bénard convection. C_ν and C_α are determined, as in model A, with the dynamic procedure. I have applied this model to internally heated channel convection.

D. The "Schumann" model has c_1 and c_2 taken as constants (2.5 and 3.0, respectively, which are near Schumann's (1991) best values for the LES of planetary boundary layers). C_ν and C_α are determined, as in model A, with the dynamic procedure. This model has been applied to high-Pr internally heated channel convection.

2.2.2 LES of Rayleigh-Bénard convection

Large eddy simulations of Rayleigh-Bénard convection were performed with a spectral-finite difference code (Piomelli *et al.*, 1987) with the dynamic SGS model using base models A and B, the same filters as described in §2.1, and a mesh of $32 \times 63 \times 32$. The molecular Prandtl number Pr was taken as 0.71 (air), and Rayleigh numbers $\mathrm{Ra} = 8|\boldsymbol{\beta}\Delta\Theta|\delta^3/\nu\alpha$ (where $\Delta\Theta$ is the wall-to-wall mean potential temperature difference) of 6.25×10^5, 2.5×10^6, and 1×10^7 were considered with horizontal-to-vertical aspect ratios of 5, 6, and 7, respectively.

The buoyant (B) base model was found to give very similar results to the scalar (A) base model without buoyancy production terms. This probably happened because the buoyancy term is generally less than, or at best comparable, to the strain term in (3) for this flow and because even with a different scaling the dynamic eddy viscosities and diffusivities tend to adjust to a similar level. The dynamic SGS model with the buoyant base model typically required only 2 or 3 iterations to determine the eddy coefficients consistently; this still doubled the computational

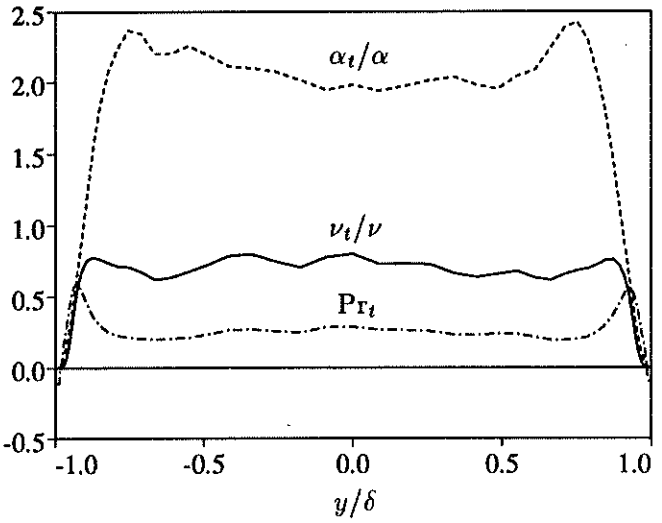

FIGURE 2. SGS eddy coefficients and Prandtl number from the LES of Rayleigh-Bénard convection with $\mathrm{Ra} = 1 \times 10^7$ and $\mathrm{Pr} = 0.71$ using the dynamic SGS model.

cost of the SGS model and, considering the little difference it made to the results, is probably not warranted. Occasionally the iteration scheme failed to find solutions at some planes, perhaps indicating that no real solutions existed. The scheme gave up after 10 iterations; but converged solutions were always found a few time steps later as flow conditions changed.

The SGS eddy viscosity and diffusivity using base model B are shown in Figure 2 with respect to their molecular values for the $\mathrm{Ra} = 1 \times 10^7$ case. Their fairly low values (of order 1 in the core) are a result of trying to resolve a reasonable amount of horizontal small scales near the wall. The dissipation due to the SGS model is comparable to that from the large scales in the core of the flow but becomes negligible near the wall. In fact, the eddy viscosity usually has small negative values in the viscous boundary layer though this has virtually no effect on the convective flow; it is not known if this is a real physical feature or an artifact of the poor horizontal resolution there. In contrast, the heat flux carried by the SGS model terms is negligible in the core of the flow but typically 20–30% of the total near the walls, which will affect the heat flux statistics. A concern is that the test filtering in the dynamic SGS model may not give accurate results near the wall since it usually samples in the energy-bearing part of the energy spectra there. The SGS Prandtl number is also shown in Figure 2. It is less than the standard value of about 0.4 (Eidson, 1985) in the core, where I find values of 0.20–0.25, but it becomes larger near the walls, reaching 0.6. Sullivan & Moeng (1992) found qualitatively similar results for Pr_t in an *a priori* test of a DNS field but at levels 3–4 times higher. They used, however, an effective filter width ratio of 4 (versus my $2^{2/3}$) and $\mathrm{Pr} = 1$; they also revamped the dynamic procedure in a way that gives only positive values of ν_t, so a direct comparison is difficult.

Large-scale statistics (such as rms velocity and potential temperature fluctuation intensities and velocity-temperature correlations) were found to be in good agreement with experimental measurements in air by Deardorff & Willis (1967) and Fitzjarrald (1976) and with previous LES results by Eidson (1985). The Nusselt numbers ($\mathrm{Nu} = 2\delta|\nabla\Theta|_w/\Delta\Theta$) of 7.7, 12.0, and 18.0 found for $\mathrm{Ra} = 6.25 \times 10^5$, 2.5×10^6, and 1×10^7 using the scalar (A) base model are about 5–10% higher than the experimental values reported by Fitzjarrald (1976) ($\mathrm{Nu} \approx 0.13\mathrm{Ra}^{0.30}$ in air) and Threlfall (1975) ($\mathrm{Nu} \approx 0.178\mathrm{Ra}^{0.280}$ in gaseous helium). A DNS for $\mathrm{Ra} = 6.25 \times 10^5$ with the same code gave $\mathrm{Nu} = 7.2$. A coarse DNS needs to be performed for one or more of these cases to determine the actual extent to which the SGS model improves the results.

2.2.3 LES of internally heated channel convection

Turbulent channel convection in water ($\mathrm{Pr} \approx 6$) with uniform volumetric heat sources and cooled, no-slip walls has been examined experimentally by Kulacki & Goldstein (1972) and numerically by Grötzbach (1982). This flow is asymmetric about the midchannel: the upper part of the channel is convectively unstable and the lower part is stable. The convective heat flux in the fully developed flow is typically downgradient in the exterior regions and countergradient in the interior. Because of this inherent asymmetry, the LES of this flow is expected to be more sensitive to the SGS model; it also allows us to test the behavior of the dynamic SGS model in transition from unstable to stable regions.

Large eddy simulations were performed with a spectral-Chebyshev code (Kim *et al.*, 1987) for $\mathrm{Pr} = 0.2$ at $\mathrm{Ra} = 1.25 \times 10^5$ on a $32 \times 65 \times 32$ mesh and at $\mathrm{Ra} = 1.25 \times 10^6$ on a $32 \times 129 \times 32$ mesh, and for $\mathrm{Pr} = 6.0$ at $\mathrm{Ra} = 1.25 \times 10^5$ on a $32 \times 65 \times 32$ mesh. Here $\mathrm{Ra} \equiv |\beta|\dot{q}\delta^5/\alpha^2\nu$, where $\dot{q}$ is the thermometric heating rate. All simulations used a horizontal-to-vertical aspect ratio of 4.

For the low-Pr runs, I used both the scalar (A) and buoyant (B) base models in the dynamic SGS model. Although there were some differences in the ν_t and α_t profiles for the low-Ra runs using different base models, the large-scale statistics were not particularly distinguishable. They shared the traits of having negative values of ν_t and/or α_t near the walls; and Pr_t had values of 0.1–0.2 in the upper convective region, growing to values near unity near the unstable upper wall and the lower, stable region. Nusselt numbers at the upper wall were found to be about 5% greater than in DNS results (O. Hubickyj & W. Cabot, unpublished). The profiles of ν_t and α_t with respect to molecular values and Pr_t are shown for the high-Ra case in Figure 3 using the buoyant (B) base model in the SGS model. Except in the narrow viscous boundary layers, ν_t and α_t are positive. In the core convective region ($y/\delta = -0.25$ to 0.75), Pr_t is about a constant 0.2 but grows to values of 1–2 in the near-upper-wall region and the stable lower channel. The eddy diffusivity remains positive throughout the center of the channel where the large-scale heat flux is countergradient; this means that the SGS heat flux is downgradient in this region, counter to the large-scale flow, and that α_t acts rather to dissipate thermal fluctuations. Since the vertical temperature gradient is small in the central region, however, the SGS heat flux is negligible there and only becomes significant in the

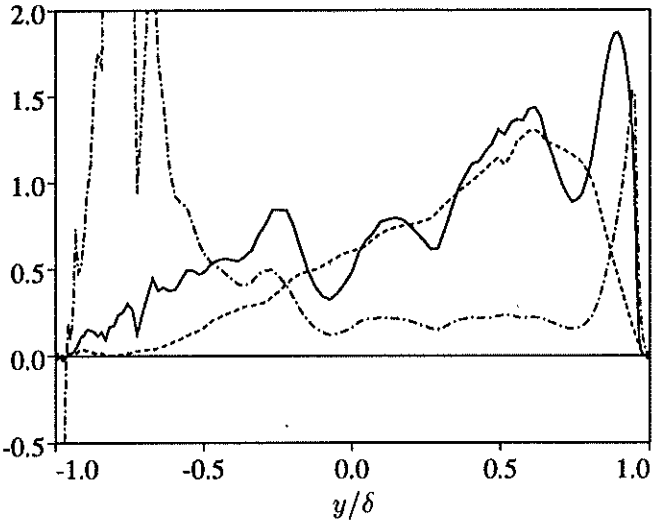

FIGURE 3. SGS eddy coefficients and Prandtl number from the LES of internally heated channel convection with $\mathrm{Ra} = 1.25 \times 10^6$ and $\mathrm{Pr} = 0.2$ using the dynamic SGS model with the buoyancy base model. —— ν_t/ν, ---- α_t/α, —·— Pr_t.

near-upper-wall region, attaining 20-30% of the total heat flux as in the LES of Rayleigh-Bénard convection. The Nusselt numbers for this case are found to be about 10% higher than DNS results. (The large-scale statistics were again found to be fairly insensitive to the base model used.)

The LES with the buoyancy base model experienced significant iteration problems, most noticeable in the low-Pr, high-Ra run. Not only were there instances of failure to converge to a solution at some planes, more disturbingly there were clear instances when more than one solution existed and the values to which Pr_t converged depended on the initial guess. (I needed to average the initial guesses over adjacent planes to get reasonable answers.) On the other hand, the LES with the scalar base model gave a broad drop in ν_t in the upper convective region, in poor agreement with the previous model (see Figure 4). Better agreement was found using the Eidson (C) base model, which includes the buoyancy production term in a less consistent but cheaper way than the buoyancy base model. The choppiness in ν_t in Figure 4 may be due in part to some numerical instability from advancing the SGS terms explicitly in the code at too large a time step, but it may also stem from filtering only in planes and not in the vertical direction, which would probably smooth the results considerably.

For direct comparison with laboratory experiments, simulations with $\mathrm{Pr} = 6$ have been recently undertaken. The eddy diffusivities from the $\mathrm{Ra} = 1.25 \times 10^5$ run using the Eidson (C) base model are shown in Figure 5a. The eddy viscosity and Pr_t are found to be negligible everywhere since the velocity in this case is almost completely resolved. However, near the upper wall I find $\mathrm{Pr}_t \approx 5$–7 (comparable to Pr). The eddy diffusivity in this case does have negative values in part of the

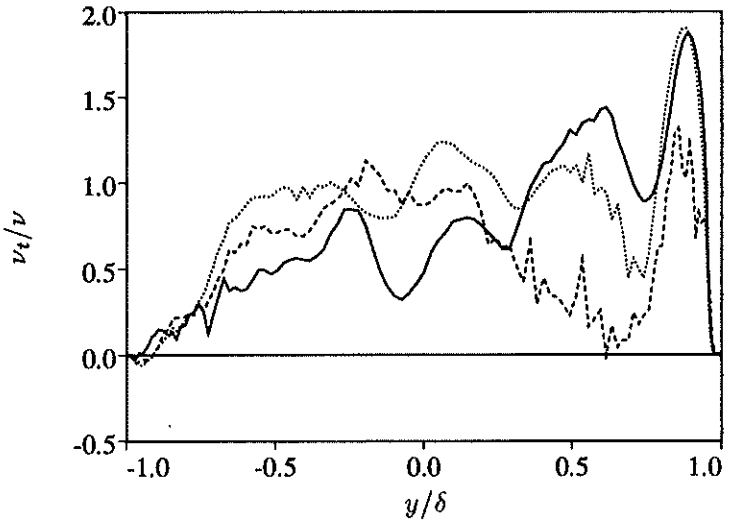

FIGURE 4. SGS eddy viscosity from the LES of internally heated channel convection with Ra = 1.25×10^6 and Pr = 0.2 using the dynamic SGS model with base model ---- A (scalar), —— B (buoyancy), and ····· C (Eidson).

central, countergradient region. Results using the Schumann (D) base model are also shown in Figure 5; α_t in this case is defined as $-\mathbf{h} \cdot \nabla\theta / \nabla\theta \cdot \nabla\theta$. Some minor differences in the central, countergradient region are noticeable. The residual heat flux resulting from these two models are shown in Figure 5b. It is seen that the Eidson base model only contributes to the heat flux in the upper convective region where the temperature gradient is appreciable while the Schumann base model contributes to the heat flux farther into the central region and gives comparatively more heat flux in the upper convective region due to the additional buoyancy term in Equation (2). Note that the SGS terms virtually vanish in the lower wall region where the flow becomes nearly laminar and that the dynamic SGS model allows a smooth transition between the turbulent and laminar regions. The LES results again tend to overestimate the Nusselt numbers by about 5% compared to DNS results; preliminary results indicate that coarse DNS computed on the same grid as LES overestimates Nu by more than twice as much. There is some discrepancy between experimental results (Kulacki & Goldstein, 1972) and numerical results (see Grötzbach, 1982), the former tending to give smaller Nusselt numbers and larger mean potential temperatures, the latter shown in Figure 6. The two different DNS results agree well but lie well below the experimental results; the LES results lie slightly below the DNS results (which make a fairer comparison).

2.2.4 Conclusions from LES results

The dynamic SGS model has been used in the LES of a number of buoyancy-driven flows with different eddy viscosity/diffusivity base models that do or do not include buoyancy terms. I tentatively conclude from the results so far that the

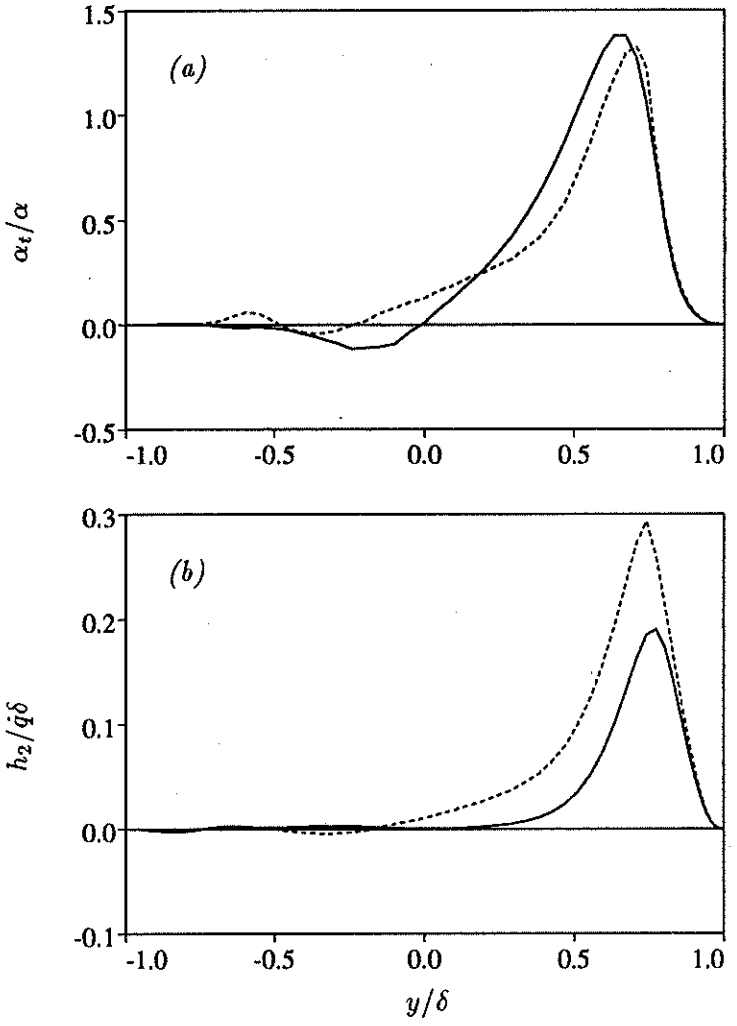

FIGURE 5. SGS (a) eddy diffusivity and (b) vertical heat flux from the LES of internally heated channel convection with $\mathrm{Ra} = 1.25 \times 10^5$ and $\mathrm{Pr} = 6$ using the dynamic SGS model with base model —— C (Eidson) and ---- D (Schumann).

buoyancy base model, which requires the consistent (iterative) determination of Pr_t, is too computationally expensive and sometimes has either no real solution or multiple solutions. The "Eidson" base model, which simply sets Pr_t to a constant in the model scaling, seems to provide a cheaper alternative that generally reproduces the buoyancy model better than the scalar model. It is not clear yet that the "Schumann" base model confers any real advantage over the others although it can accommodate, in principle, the countergradient heat flux that occurs in internally heated channel convection.

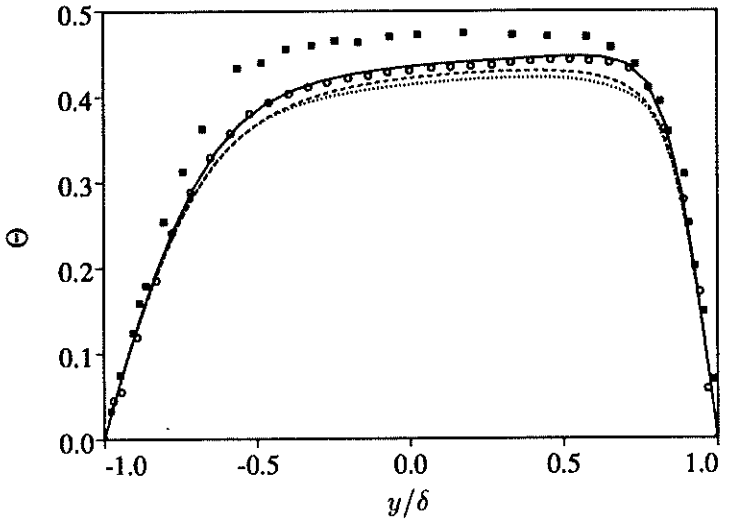

FIGURE 6. Mean potential temperature for internally heated channel convection with $\mathrm{Ra} = 1.25 \times 10^5$ and $\mathrm{Pr} = 6$. ■ experimental data (Kulacki & Goldstein, 1972), o DNS (Grötzbach, 1982), ——— DNS (O. Hubickyj & W. Cabot, unpublished), - - - - LES with base model C, and ····· LES with base model D.

2.3 DNS of fully compressible convection

Direct numerical simulations of fully compressible, internally heated channel convection were performed using a fourth-order, explicit, finite-difference code (Thompson, 1990, 1992a,b). Simulations were performed for several different density and temperature stratifications at $\mathrm{Ra} = 1.23 \times 10^5$ (defined at midchannel) and $\mathrm{Pr} = 0.2$ in a linearly varying gravity. Fixed temperature, no-stress (free-slip) boundary conditions are used at the walls. The no-stress, impermeable walls are meant to approximate free boundary conditions. For uniform volumetric heating rates, a mesh of $96 \times 33 \times 96$ and horizontal-to-vertical aspect ratios of 4 or 5 are used; for uniform specific heating rates, a mesh of $64 \times 65 \times 64$ and horizontal-to-vertical aspect ratios of 3 or 4 are used.

The mean potential temperature profile from a low stratification, low Mach number run was found to agree very well with the Boussinesq results of Cabot *et al.* (1990) for nearly the same values of Ra and Pr. For moderate to large density stratifications (central to wall ratios of a few to greater than 10) and moderate temperature stratification, the convection was found to be weaker due to the increase in viscosity and diffusivity (with inverse density) toward the walls; the Nusselt number was found to vary approximately as $\mathrm{Nu} - 1 \propto (\mathrm{Ra}^{1/4} - \mathrm{Ra}_c^{1/4})(\rho_w/\rho_c)^{3/4}$, where $\mathrm{Ra}_c \sim 1000$ is the critical Rayleigh number for the onset of convection. The interior rms Mach number was found to be typically 0.20–0.25, increasing to about 0.4 at the free-slip walls. Peak Mach numbers were found to be about 2.5 times the rms, and Mach numbers slightly in excess of unity were observed at the walls

in agreement with previous simulations by Malagoli *et al.* (1990). The compressible code did not require an additional high-order artificial damping built into it to compute these runs. Only weak shock features appeared to form because the high speed flows that form as the hot, rising interiors of convective cells expand horizontally along the walls tend to impinge on neighboring cells obliquely as the convergent flows plunge downward in cool, narrow downdrafts. Even a simulation with high temperature stratification (with central to wall ratio of ~ 30) with peak Mach numbers at the walls of 3.8 and occasional strong shock fronts was able to run a fair length of time without the artificial dissipation to damp two-delta waves, although it was eventually needed in this case.

The levels of fluctuations in thermodynamic quantities relative to their mean values are found to be consistent with those of Chan & Sofia (1989) for simulations of deep stellar convection. As in their work, the rms pressure fluctuations were found to be almost equal to the turbulence kinetic energy everywhere in the convective region so that the relative pressure fluctuations scale as rms Mach number squared. An examination of the terms in the equation governing the potential energy $P = \overline{p'^2}/2\gamma\overline{p}$ shows that they typically satisfy some of Zeman's (1991) assumptions for a compressible boundary layer. The steady-state equation for P gives

$$\underbrace{-(\overline{\mathbf{u}}\cdot\nabla P + 2\gamma P\nabla\cdot\overline{\mathbf{u}} + \frac{P}{\overline{p}}\overline{\mathbf{u}}\cdot\nabla\overline{p})}_{1} \underbrace{-\overline{p'\nabla\cdot\mathbf{u}'}}_{2} \underbrace{-\frac{1}{\gamma\overline{p}}\overline{p'\mathbf{u}'}\cdot\nabla\overline{p}}_{3}$$
$$\underbrace{-\frac{1}{\gamma\overline{p}}(\overline{p'\mathbf{u}'\cdot\nabla p'} + \gamma\overline{p'^2\nabla\cdot\mathbf{u}'})}_{4} + \underbrace{(\gamma-1)\frac{\overline{H'p'}}{\gamma\overline{p}}}_{5} = 0\,. \tag{4}$$

Here H is the net heating rate for the internal energy. As shown in Figure 7, term 3 is a production term due to the pressure flux, which is very nearly balanced by the pressure dilatation in term 2. The remaining terms are higher order in Mach number squared and are negligible in moderate Mach number flows. Even in the high Mach number case cited previously, term 2 cancelled 60% of term 3. The production in term 3 is controlled here primarily by buoyancy terms since the pressure flux is proportional to the convective heat (enthalpy) flux and the pressure gradient is proportional to gravity from hydrostatic equilibrium. For convection then, unlike Zeman's compressible boundary layer, the pressure flux should be modeled in terms of a thermal convection model, perhaps using the superadiabatic temperature gradient, rather than in terms of the normal density gradient.

Compressional effects only appear to be significant at the (artificial) walls in the fully convective channels. Simulations with uniform specific heating rates are currently under way that feature convectively stable exterior regions bounding a convective interior. These should provide a better basis for determining compressional effects in the freely bounded convection; it is likely that acoustic effects are more important in the convectively stable exterior. We are also currently exploring whether the use of soundproofed, pseudo-compressible governing equations (like

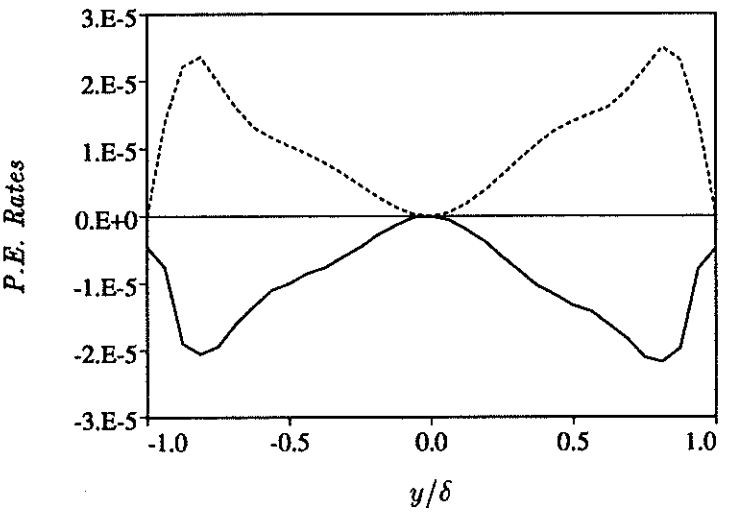

FIGURE 7. Potential energy rates from equation (4) in fully compressible channel convection with high density stratification: —— pressure dilatation (term 2) and ---- pressure flux production (term 3).

Durran, 1989) in the simulations of highly stratified convection would be acceptably accurate and more efficient than the fully compressible simulations.

3. Future plans

3.1 "One-equation" local dynamic subgrid-scale models in channel flow

Using locally defined coefficients from the dynamic SGS model has generally led to numerical instability due to persistent negative values of the SGS eddy viscosity. Ghosal, Lund & Moin in this volume (also see Wong, 1992) have proposed scaling the eddy viscosity with half of the trace of SGS residual stress ($k = \tau_{kk}/2$), which is evolved along with the flow. If the local k is driven to zero by negative eddy viscosities, the local eddy viscosity vanishes until k is replenished. This limits the duration of negative eddy viscosities and has been shown to stabilize calculations of homogeneous turbulence with local dynamic SGS modeling. We plan to implement this approach in channel flow. We also plan to implement Ghosal *et al.*'s variational approach to determine the local dynamic coefficients consistently.

An immediate problem arises in how to cast the k-equation to give proper behavior near and at the walls. Ghosal *et al.* use the form of a standard one-equation k-model with a SGS production term to evolve k at the grid-filter ($\bar{}$) level:

$$Dk/Dt = \nu_t \bar{S}^2 + \nabla \cdot [(\nu + \nu_D)\nabla k] - C_E k^{3/2}/\Delta\,, \tag{5}$$

where $\nu_t = C\Delta k^{1/2}$ is determined by the dynamic test-filtering procedure (in which C is determined locally) and $\nu_D = C_D \Delta k^{1/2}$ is the diffusive eddy viscosity. The constants or coefficients C_D and C_E remain to be specified; they could be preset

constants or be themselves determined by a dynamic fitting procedure. First, k properly goes to zero at a no-slip wall as y_w^2 (where y_w is the distance from the wall). Since (5) is a second-order equation, only two boundary conditions are needed, namely $k = 0$ at either wall, but this generally results in $k \propto y_w$ at the walls. Second, the $\nu\nabla^2 k$ term is generally finite at the wall, but it is difficult to make any other term in (5) balance it for plausible definitions of Δ, C_D, and C_E. (Note that ν_t in (5) always goes as y_w^3 from the dynamic model.) Both of these problems can be addressed (but not necessarily solved) if we consider evolving the equation for q (where $k = q^2/2$) and understand the last term in (5) to be the model for the reduced dissipation rate $\varepsilon'' = \varepsilon - \nu\nabla q \cdot \nabla q$, which goes as y_w^2 at the wall. The additional term $\nu\nabla q \cdot \nabla q$ must then be subtracted from $\nu\nabla^2 k$ in (5) to give $\nu q\nabla^2 q$, and the q-equation conveniently becomes

$$Dq/Dt = c\Delta\overline{S}^2 + \nabla \cdot [(\nu + c_d\Delta q)\nabla q] + c_d\Delta\nabla q \cdot \nabla q - c_e q^2/\Delta\,. \tag{6}$$

The lower case constants/coefficients in (6) differ from their upper case counterparts in (5) by various powers of $\sqrt{2}$. Note that there is an additional source term in (6) from the diffusion term in (5). But now the term $\nu\nabla^2 q$ is generally finite and unbalanced at the walls (unless, e.g., $c_d\Delta$ in the diffusive terms is made finite at the walls). However, even if this term is not balanced at the wall (in which case the numerical solution gives $q = \partial^2 q/\partial y^2 = 0$), one obtains the correct second-order asymptotic behavior for k at the wall ($k = \partial k/\partial y = 0$).

Tests of the sensitivity of the results to different treatments of the k- or q-equation will need to be made for the LES of channel flow. A further modification that has been made to the channel flow code is to use top-hat (real space averaging) filters in the horizontal directions to assure that the trace of the residual SGS stress at the test-filter level is positive definite (which is not necessarily the case for spectral-cutoff filters). Also, top-hat filtering will also eventually be implemented in the direction normal to the walls for consistency with simulations of homogeneous flows, albeit not strictly commutative with normal derivatives on the stretched grid used. It also appears that a scheme must be developed for treating points with vanishing or negative q since equation (6) may have realizability problems.

3.2 Further testing of the dynamic SGS model in thermal convection problems

More large eddy simulations of Rayleigh-Bénard and internally heated channel convection are needed to determine the optimal values of c_1 and c_2 in equations (1)–(3) for the base models of the dynamic SGS model with plane averaging. The computational expense of computing them consistently at each time step with the dynamic test-filtering procedure is prohibitive (and ill-defined at some points), but sample calculations might be used to establish reasonable constant or functional values. For example, the value of $\mathrm{Pr}_t = 1/c_1$ is found to about a constant 0.2 in the core of several convective flows when $c_2 = 0$ (although this may be a function of filter sizes and the molecular Prandtl number). Some corresponding coarse-grid direct numerical simulations are also needed to gauge the effect of the SGS models. Filtering in the vertical direction, not explicitly done heretofore in the channel codes,

will also be implemented. Results from these volume-filtered channel simulations will be compared with previous DNS and plane-filtered LES results. The effect of including Leonard stress terms, similar to the mixed Smagorinsky-Bardina model (Piomelli *et al.*, 1987), will also be tested; these terms are generally non-dissipative but provide a fairly realistic level of local forward and backward scatter.

More general base models for the subgrid scales are possible, especially in more complicated flows (e.g., with both buoyancy and rotation). Such models are being considered based on the governing equations for the residual Reynolds stress and heat flux, which closely resemble Reynolds stress equations for large-scale modeling (cf. Schumann, 1991). Dropping material derivative and diffusion terms, the governing equations for residual stress ($\boldsymbol{\tau}$), heat flux ($\mathbf{h}$), and temperature intensity squared (k_θ) are

$$\mathcal{A}\cdot\boldsymbol{\tau}+\boldsymbol{\tau}\cdot\mathcal{A}^\dagger+\boldsymbol{\beta}\mathbf{h}+\mathbf{h}\boldsymbol{\beta}=\boldsymbol{\Pi}-2\boldsymbol{\varepsilon}\,, \tag{7}$$

$$\boldsymbol{\tau}\cdot\nabla\theta+\mathcal{A}\cdot\mathbf{h}+\boldsymbol{\beta}k_\theta=\boldsymbol{\Pi}_\theta-2\varepsilon_\theta\,, \tag{8}$$

$$\mathbf{h}\cdot\nabla\theta=-\varepsilon_{\theta\theta}\,, \tag{9}$$

where $\mathcal{A}$ comprises the velocity gradient tensor and the mean rotation tensor ($A_{ij}=u_{i,j}-2\Omega_\ell\epsilon_{ij\ell}$) and $\mathcal{A}^\dagger$ is its transpose. The right-hand sides of (7)–(9) involve pressure-strain terms (Π) and dissipation terms (ε) that must be modeled. A Smagorinsky model-like equation (1), for example, is recovered from (7) for standard return-to-isotropy models of $\boldsymbol{\Pi}$ and approximating the trace-free part of the left-hand side by $2\tau_{kk}\mathbf{S}/3$. The importance of the more general terms will be tested in *a priori* tests of DNS data. The need for explicit rotational terms in the dynamic SGS base model will be tested with the LES of some rotating flows. A base model with rotational effects might be based on the above equations with rotation entering through $\mathcal{A}$ and/or through the models for Π and ε.

The net amount of energy and dissipation that the dynamic SGS model can represent in channel flow has been limited due to the reduction of both normal and horizontal length scales near the no-slip walls, which causes the test filter to eliminate scales with a significant fraction of energy. Large eddy simulations for channel convection with no-stress walls will be performed in an attempt to improve on this situation. However, only flows with smaller scale disparity (freely bounded or with matching to near-wall solutions) will probably be able to use the dynamic SGS model efficiently at very high Reynolds numbers. Finally, we plan to implement the dynamic SGS model in our compressible convection simulations, starting with the form used in the LES of homogeneous compressible flow by Moin *et al.* (1991). The simulations now in progress with convectively stable exterior regions freely bounding the interior convective region should be more suitable for the dynamic SGS model by eliminating (or at least severely reducing) the amount of turbulence at the impermeable walls.

REFERENCES

CABOT, W. 1991 Large eddy simulations of passive and buoyant scalars with dynamic subgrid-scale models. In *CTR Annual Research Briefs 1991*, ed. P. Moin,

W. C. Reynolds, & J. Kim (Center for Turbulence Research, Stanford University/NASA Ames), pp. 191–205.

CABOT, W., & MOIN, P. 1991 Large eddy simulation of scalar transport with the dynamic subgrid-scale model. *CTR Manuscript 128,* (Center for Turbulence Research, Stanford University/NASA Ames). Also to appear (1992) in *Large Eddy Simulation of Complex Engineering and Geophysical Flows*, ed. B. Galperin & S. A. Orszag (Cambridge University Press).

CABOT, W., POLLACK, J. B., CASSEN, P., HUBICKYJ, O., & CANUTO, V. M. 1990 Direct numerical simulations of turbulent convection: I. Variable gravity and uniform rotation. *Geophys. Astrophys. Fluid Dyn.* **53,** 1–42.

CHAN, K. L., & SOFIA, S. 1989 Turbulent compressible convection in a deep atmosphere. IV. Results of three-dimensional computations. *Astrophys. J.* **336,** 1022–1040.

DEARDORFF, J. W., & WILLIS, G. E. 1967 Investigation of turbulent thermal convection between horizontal plates. *J. Fluid Mech.* **28,** 675–704.

DURBIN, P. A. 1992 On modeling three-dimensional wall layers. *CTR Manuscript 135,* (Center for Turbulence Research, Stanford University/NASA Ames).

DURRAN, D. R. 1989 Improving the anelastic approximation. *J. Atmos. Sci.* **46,** 1453–1461.

EIDSON, T. M. 1985 Numerical simulation of turbulent Rayleigh-Bénard convection using subgrid scale modeling. *J. Fluid Mech.* **158,** 245–268.

FITZJARRALD, D. E. 1976 An experimental study of turbulent convection in air. *J. Fluid Mech.* **73,** 693–719.

GERMANO, M., PIOMELLI, U., MOIN, P., & CABOT, W. H. 1991 A dynamic subgrid-scale eddy viscosity model. *Phys. Fluids A.* **3,** 1760–1765.

GRÖTZBACH, G. 1982 Direct numerical simulation of the turbulent momentum and heat transfer in an internally heated fluid layer. In *Heat Transfer 1982*, vol. 2, ed. U. Grigull, E. Hahne, K. Stephan & J. Straub (Hemisphere Publishing), pp. 141–146.

KIM, J., MOIN, P., & MOSER, R. 1987 Turbulence statistics in fully developed channel flow at low Reynolds number. *J. Fluid Mech.* **177,** 133–166.

KULACKI, F. A., & GOLDSTEIN, R. J. 1972 Thermal convection in a horizontal fluid layer with uniform volumetric energy sources. *J. Fluid Mech.* **55,** 271–287.

LILLY, D. 1992 A proposed modification of the Germano subgrid-scale closure method. *Phys. Fluids A.* **4,** 633–635.

MALAGOLI, A., CATTANEO, F., & BRUMMELL, N. H. 1990 Turbulent supersonic convection in three dimensions. *Astrophys. J.* **361,** L33–L36.

MASON, P. J. 1989 Large-eddy simulation of the convective atmospheric boundary layer. *J. Atmos. Sci.* **46,** 1492–1516.

MOIN, P., SHIH, T.-H., DRIVER, D., & MANSOUR, N. N. 1990 Direct numerical simulations of a three-dimensional turbulent boundary layer. *Phys. Fluids A.* **2**, 1846–1853.

MOIN, P., SQUIRES, K., CABOT, W., & LEE, S. 1991 A dynamic subgrid-scale model for compressible turbulence and scalar transport. *Phys. Fluids A.* **3**, 2746–2757.

NIEUWSTADT, F. T. M. 1990 Direct and large-eddy simulation of free convection. In *Heat Transfer 1990*, vol. 1, ed. G. Hetsroni (Hemisphere Publishing), pp. 37–47.

PIOMELLI, U., FERZIGER, J. H., & MOIN, P. 1987 Models for large eddy simulations of turbulent channel flows including transpiration. *Rep. TF-32, Dept. of Mech. Eng.* (Stanford University).

SCHUMANN, U. 1991 Subgrid length-scales for large-eddy simulation of stratified turbulence. *Theoret. Comput. Fluid Dyn.* **2**, 279–290.

SMAGORINSKY, J. 1963 General circulation experiments with the primitive equations. I. The basic experiment. *Mon. Weather Rev.* **91**, 99–164.

SULLIVAN, P. P., & MOENG, C.-H. 1992 An evaluation of the dynamic subgrid scale model in buoyancy driven flows (to be published).

THOMPSON, K. W. 1990 Turbulent transport in the solar nebula. In *CTR Annual Research Briefs 1989*, ed. P. Moin, W. C. Reynolds, & J. Kim (Center for Turbulence Research, Stanford University/NASA Ames), pp. 175–184.

THOMPSON, K. W. 1992a Numerical conservation properties of finite difference approximations. Submitted to *J. Comp. Phys.*

THOMPSON, K. W. 1992b High-order dissipation methods for the suppression of high-frequency numerical oscillations. Submitted to *J. Comp. Phys.*

THRELFALL, D. C. 1975 Free convection in low-temperature gaseous helium. *J. Fluid Mech.* **67**, 17–28.

WONG, V. C. 1992 A proposed statistical-dynamic closure method for the linear or nonlinear subgrid-scale stresses. *Phys. Fluids A.* **4**, 1080–1082.

ZEMAN, O. 1991 The role of pressure-dilatation correlation in rapidly compressed turbulence and in boundary layers. In *CTR Annual Research Briefs 1991*, ed. P. Moin, W. C. Reynolds, & J. Kim, (Center for Turbulence Research, Stanford University/NASA Ames), pp. 105–117.